The Aerodynamics of a Diabolo

Darren Jia[1] Fei Liu[2]

July 20, 2021

Abstract

Diabolo is a popular game in which the object can be spun up to speeds of 5000 rpm. This high spin velocity gives the diabolo the necessary angular momentum to remain stable. The shape of the diabolo generates interesting air flow pattern. The viscous air applies an resistive torque on the fast spinning diabolo. Through computational fluid dynamics (CFD) simulation it's shown the resistive torque has an interesting dependence on the angular speed of the diabolo. Further, the geometric shape of the diabolo affects the dependence of torque on angular speed.

1 Introduction

The aerodynamics around spinning objects has long been studied using CFD and experimental techniques due to its complexity and a lack of analytical solution for the turbulent nature of flows involved. Objects of particular interest include cylinders [Kim] and spheres [2] [3] [4]. Improved understanding of the aerodynamics of a spinning and moving spherical objects lends to better design of sports objects such as cricket balls [5], golf balls [6], [7], [8], and soccer balls [9], [10], [11], and [12]. For example, it's long been known that the dimpled surface of a golf ball [7] [8] will disrupt laminar flow around the golf ball and causes the onset of turbulent flow to happen near the leading edge of the golf ball. Such early onset of turbulent air flow significantly reduces the air resistance so the golf ball can fly further.

A traditional East Asian past time involves spinning a diabolo on a thin thread while the person performs many challenging movements. The aerodynamics aspect of a spinning diabolo has not been studied in the past. In this work, we present a set of preliminary results concerning the aerodynamics of a spinning diabolo and the relationship between the spin angular velocity of the diabolo and the torque applied on the diabolo due to air resistance.

2 Simulation Setup

The aerodynamics of a spinning diabolo is simulated using the open source CFD software OpenFOAM [13] [14] [15]. We have previously implemented a solver [16] based on finite difference methods which suffered from the problem that the grid resolution is insufficient to resolve the boundary layer behavior near the solid walls of the diabolo.

[1] *Ridge High School*
[1] *NJ Science Academy*

OpenFOAM is a popular open source CFD package that supports finite volume [13] approach to aerodynamics simulation. In addition, the finite volume of the mesh [17] is adaptive and can be refined near the walls of the diabolo to capture the details of the flow field near the wall, where a large gradient of the flow field variables is present.

To set up the simulation, we first create a geometry of the diabolo using blender (open source CAD software) [18]. Then a finite volume mesh with refinement zone near the diabolo is created to be used in the OpenFOAM solver.

2.1 Geometry of a Diabolo

We used the measurements of a Mister Babache [19] diabolo along with a reference image of a Flight Lander diabolo to create a diabolo geometry in blender as shown in figure 1.

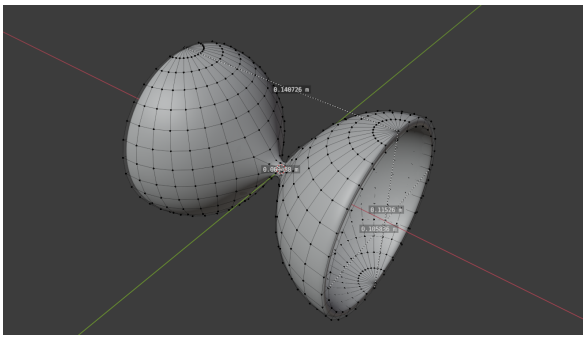

Figure 1: Geometry of the diabolo used in simulation: length 14.07cm, inner diameter 10.58 cm, outer diameter: 11.53 cm, narrow section diameter: 0.95cm

2.2 Meshing

As shown in figure 2, a refined boundary layer is formed around the wall of the diabolo. Then a refined mesh in the shape of a cylinder surrounds the diabolo. The radius of this refined mesh is about 10 cm. Finally the resolution of the mesh further away from the diabolo has a lower resolution.

On the sectional view of the mesh, the largest cells have a resolution of $6.45 * 10^{-3} \times 1.85 * 10^{-2}$ in meter, each refinement level increases the resolution by a scale of 2. Near the diabolo, the resolution becomes $3.23 * 10^{-3} \times 9.23 * 10^{-3}$ meter. Finally the boundary layer mesh has a highest resolution of $1.62 * 10^{-3} \times 4.61 * 10^{-3}$ meter. Overall the mesh has 127313 cells.

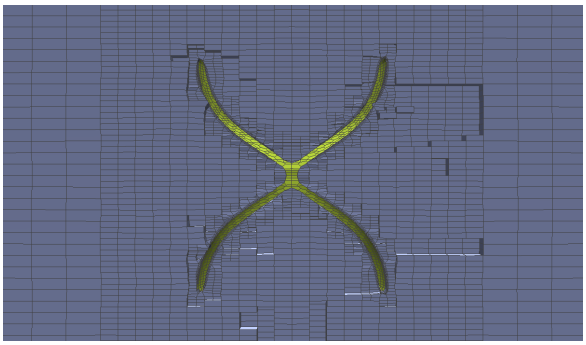

Figure 2: Meshing of the diabolo, the resolution of the mesh increases near the wall of the diabolo, including refined boundary layer on the diabolo.

2.3 Solver

OpenFOAM SIMPLE solver uses a finite volume [13] approach to solve the steady-state incompressible viscous fluid flow [14] [15]. This is a suitable algorithm for the diabolo simulation as we are looking for a flow field solution when the angular speed of the diabolo becomes steady. The governing equations of the incompressible viscous fluids are the typical incom-

pressible steady Navier-Stokes equations:

$$\nabla \vec{v} = 0 \tag{1}$$

$$\nabla \cdot (\vec{v} \otimes \vec{v}) = -\nabla p + \nabla(\nu \nabla \vec{v}) \tag{2}$$

In the SIMPLE algorithm, the pressure-velocity coupled equation is solved by decoupling the pressure and momentum fields through predictor-corrector steps. During the momentum predictor step, H matrix is solved from the momentum equation which has been matrixized on the finite volume mesh.

$$\nabla \cdot (\vec{v} \otimes \vec{v}) - \nabla(\nu \nabla \vec{v}) = -\nabla p \tag{3}$$

$$MV = -\nabla P \tag{4}$$

$$A = diag(M) \tag{5}$$

$$H = AV - MV \tag{6}$$

$$AV - H = -\nabla P \tag{7}$$

Now we can start the iterative process solving for pressure P and velocity V. Start with the momentum equation,

$$V = A^{-1}H - A^{-1}\nabla P \tag{8}$$

Substituting the V equation into continuity equation leads to a Poisson equation of pressure that can be solved by under relaxation method.

$$\nabla V = \nabla(A^{-1}H - A^{-1}\nabla P) = 0 \tag{9}$$

$$\nabla(A^{-1}\nabla P) = \nabla(A^{-1}H) \tag{10}$$

In the predictor step, the momentum equation is solved using initial pressure P and velocity boundary condition to find velocity V

$$MV = -\nabla P \tag{11}$$

The velocity field V is then used in the Poisson equation to solve pressure P

$$\nabla(A^{-1}\nabla P) = \nabla(A^{-1}H) \tag{12}$$

The pressure field is then used in equation (8) to correct V at the boundary. This is the corrector step. This process is iterated until a solution of V and P converges for the computational domain.

In this particular simulation, the $k-\epsilon$ [20] turbulence mode is enabled. The Reynolds number $Re = \frac{vL}{\nu}$ for a spinning diabolo at hundreds of rad/s teogether with the geometry we used far exceeds the laminar regime of air flow.

2.4 Flow pattern

In the pressure (Figure 4), speed (Figure 5), and vorticity (Figure 6) contour plots, we clearly observe the presence of vortex shedding with its signature wavy pattern. As the angular velocity increases, the magnitude of pressure change from reference pressure, air speed, vorticity and wall shear stress all increase. The high pressure regions at the top and bottom of the computational domain are artifacts of the simulation where the mesh cells between the rotating refinement mesh and outer boundary of the computational domain rotate relative to the refinement geometry. This artifact can be more readily seen by examining the z-component of velocity which are opposite in sign above and below the diabolo. Further, the distance between origin (center of the diabolo) and the inner boundary of the high speed region above or below is exactly the radius of the cylindrical refinement mesh. The flow field beyond the refinement mesh is not analyzed due to the artificial nature of the result from OpenFOAM in this region.

2.5 Torque

As the diabolo is spinning, air friction applies a resistive torque on the diabolo due to wall shear

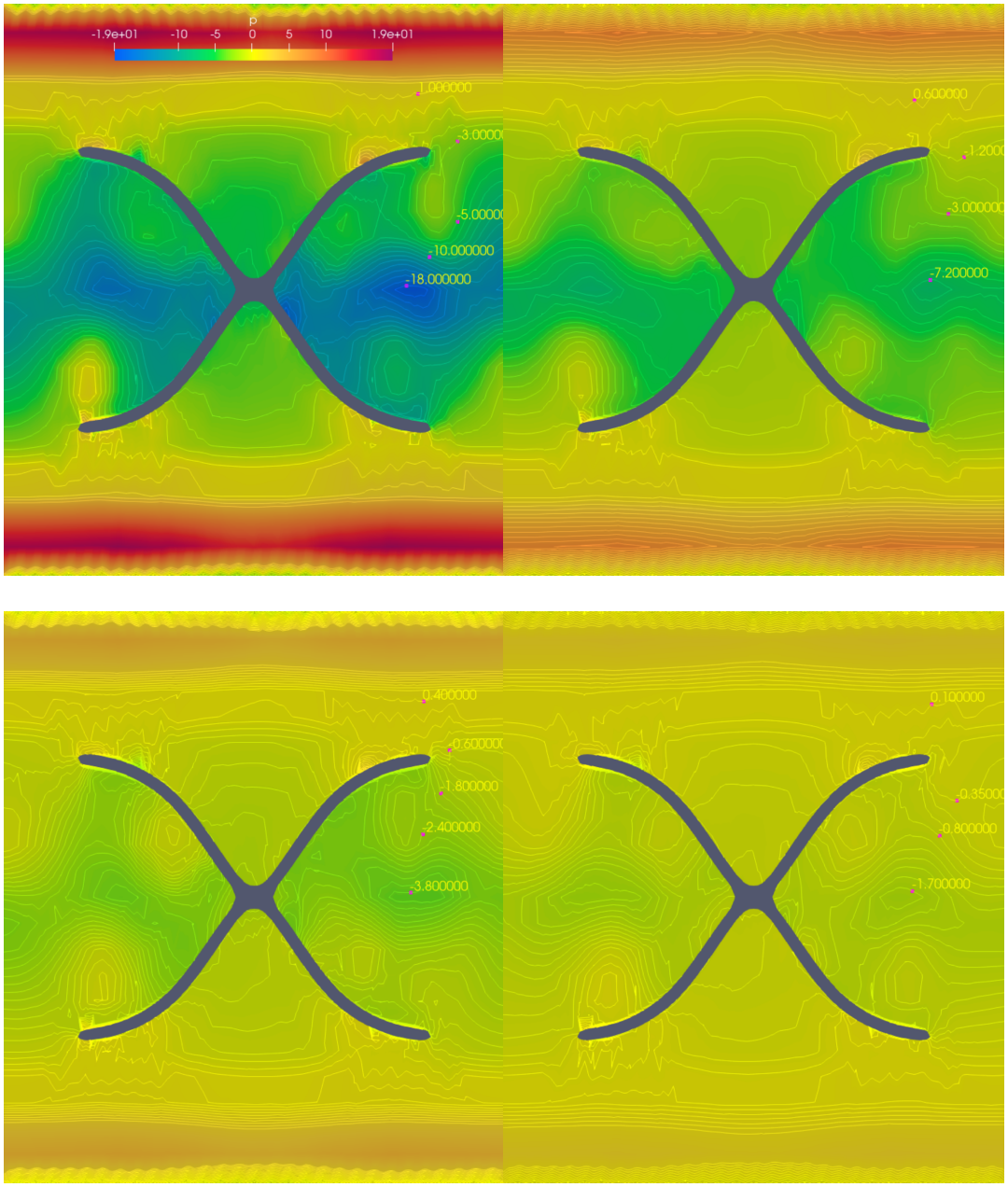

Figure 3: The pressure field around the diabolo, top left $\omega = 600$ rad/s, top right $\omega = 400$ rad/s, bottom left $\omega = 300$ rad/s, bottom right $\omega = 200$ rad/s. All diagrams use the same color scale for the range of pressure between -19 to +19 Pa.

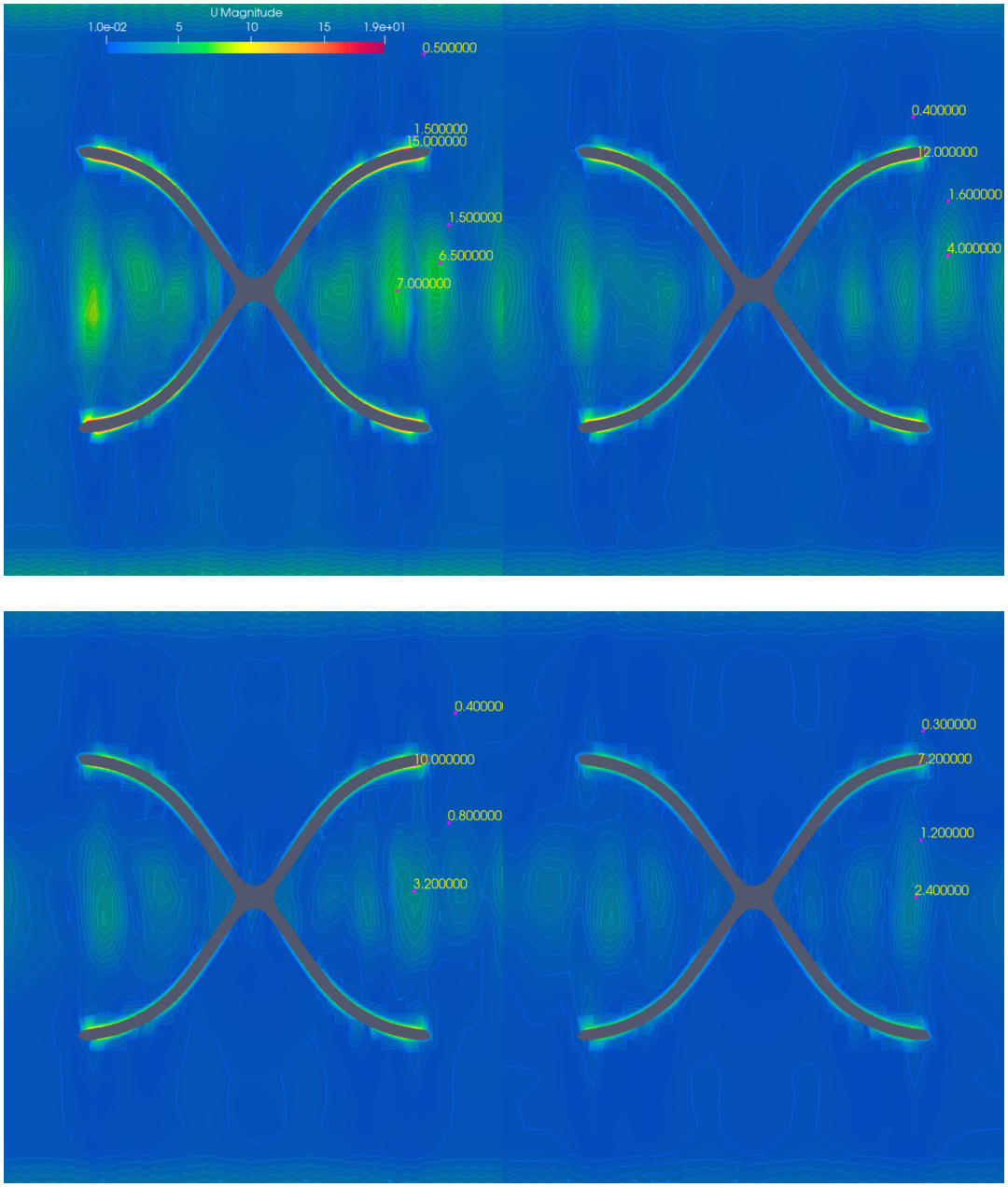

Figure 4: Air speed around the diabolo, top left $\omega = 600$ rad/s, top right $\omega = 400$ rad/s, bottom left $\omega = 300$ rad/s, bottom right $\omega = 200$ rad/s. All diagrams use the same color scale for the range of speed between 0.01 to 19 m/s.

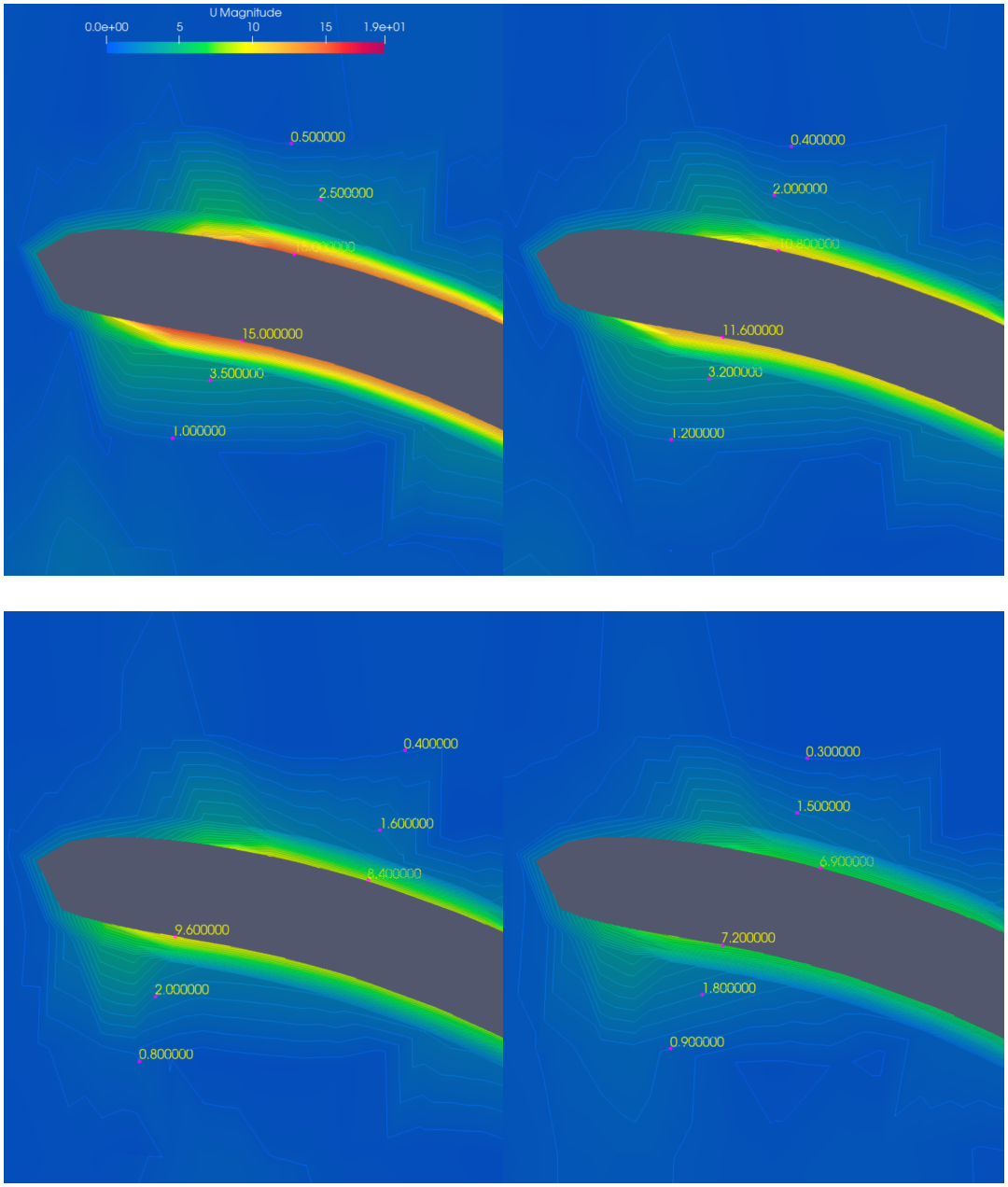

Figure 5: Air speed in the boundary layer of the diabolo, top left $\omega = 600$ rad/s, top right $\omega = 400$ rad/s, bottom left $\omega = 300$ rad/s, bottom right $\omega = 200$ rad/s. All diagrams use the same color scale for the range of speed between 0.01 to 19 m/s.

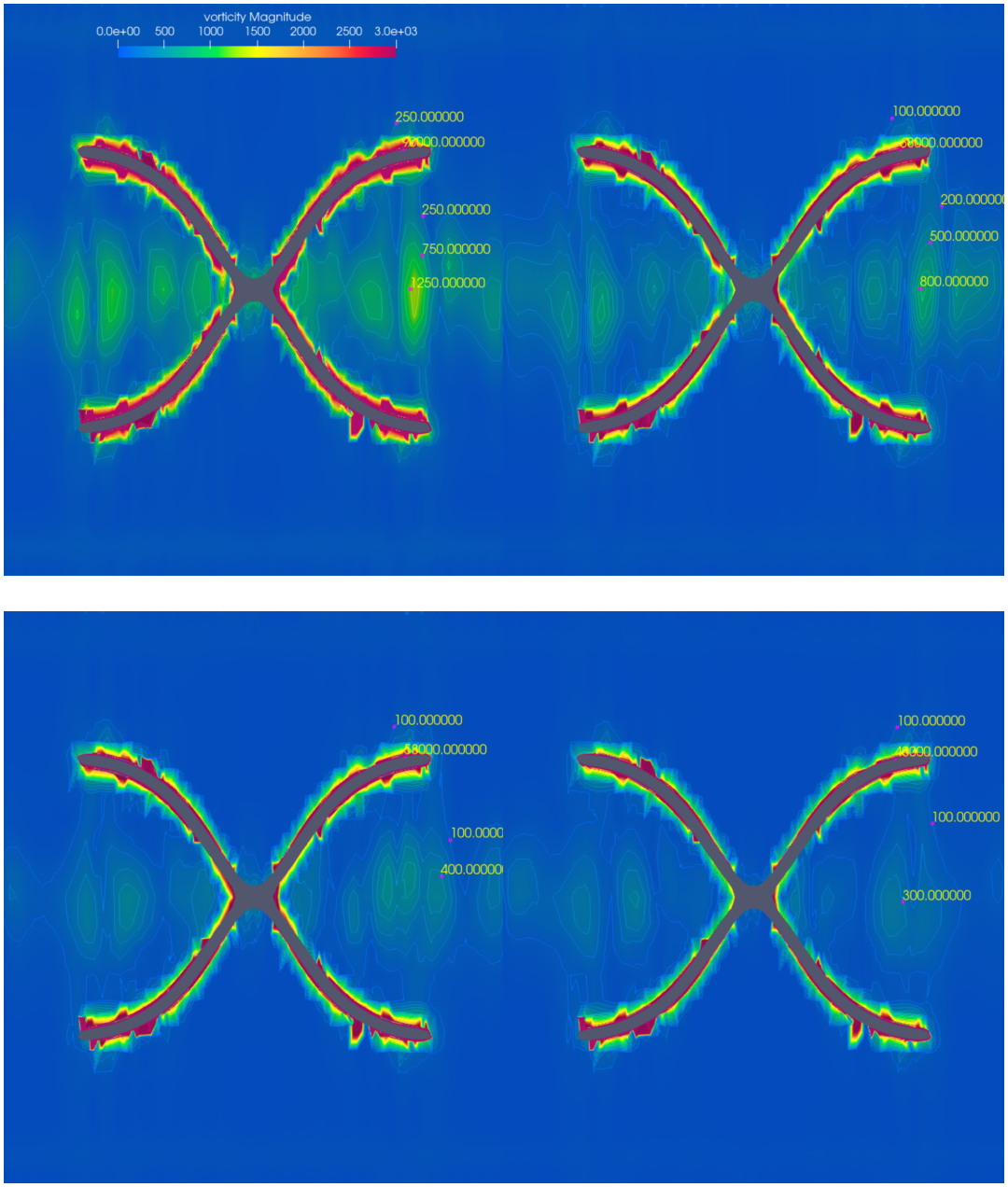

Figure 6: Vorticity around the diabolo, top left $\omega = 600$ rad/s, top right $\omega = 400$ rad/s, bottom left $\omega = 300$ rad/s, bottom right $\omega = 200$ rad/s. All diagrams use the same color scale for the range of vorticity between 0 to 3000 1/s.

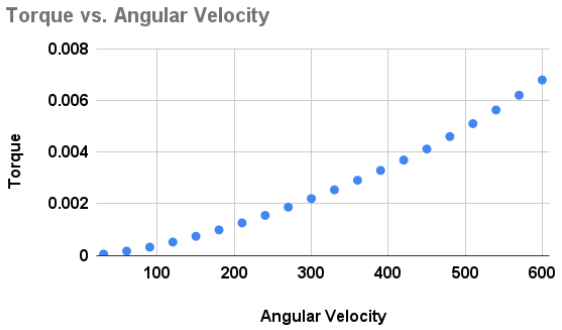

Figure 7: Torque on the base length diabolo model over varying angular velocities. As the angular velocity increases from 0 to 600 rad/s, torque increases from 0 to 0.007 Nm.

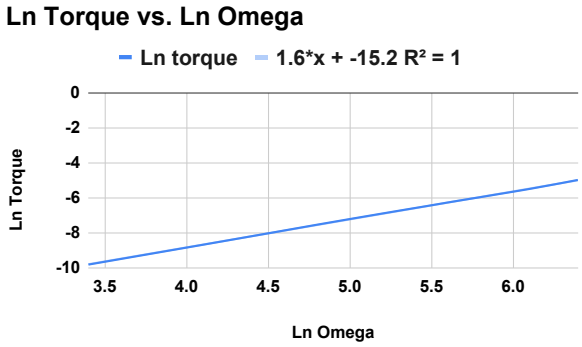

Figure 8: A log scale graph of the Torque vs ω data is shown here. Using the relationship found by the trendline, an equation can be created relating Angular Velocity and Torque. $\tau = 2.5 \cdot 10^{-7} \cdot \omega^{1.6}$.

stress. As time passes, the torque exerted on the diabolo stabilizes and converges on a value from elliptic solver in OpenFOAM, allowing us to record the torque for any given angular velocity. We simulated the diabolo rotating along its lengthwise axis between 30 rad/s and 600 rad/s with an interval of 30 rad/s between data points. Figure 7 shows how the torque calculated along this axis varies as a function of angular velocity ω based on the measured values shown in table 1. The smooth pattern of the curve suggests a power law relationship and the use of linear regression. By applying logrithmic functions of the torque and angular velocity values, we can produce the relationship $ln(\tau) = b \cdot ln(\omega) + a$. Then taking e to the power of both sides yields the following relationship

$$\tau = \alpha\omega^{\beta} \tag{13}$$

ω (rad/s)	τ (N m)
30	5.42E-05
60	1.66E-04
90	3.22E-04
120	5.17E-04
150	7.41E-04
180	9.89E-04
210	1.26E-03
240	1.55E-03
270	1.87E-03
300	2.20E-03
360	2.91E-03
390	3.29E-03
420	3.69E-03
450	4.12E-03
480	4.60E-03
510	5.10E-03
540	5.63E-03
570	6.20E-03
600	6.79E-03

Table 1: Torque calculated from wall shear stress in OpenFOAM as a function of the diabolo's spin angular velocity.

As shown figure 9, this equation correctly

models the torque found through OpenFOAM simulation with high correlation. For the base diabolo geometry, the two coefficients through regression are $\alpha = 2.5 \cdot 10^{-7}$ and $\beta = 1.6$ We first use a base diablo geometry configuration to examine the torque-angular velocity relationship. In the next section, the geometry of the diabolo is varied and the effect of geometry on the torque-angular velocity is further investigated.

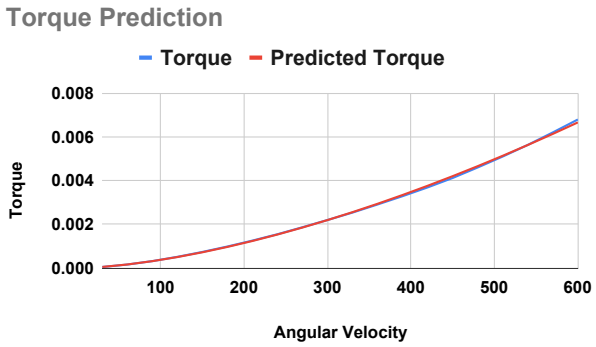

Figure 9: The simulated torque found in OpenFOAM and the predicted torque created by our equation match well.

3 Effect of geometry on aerodynamics

After establishing the power law relationship between torque and angular velocity, we now modify the base geometry of the diabolo by scaling the diabolo model. Diabolos with varying lengths are created by scaling the diabolo along its lengthwise axis, while keeping the radius of the diabolo the same. The length scales are shown in table 2. We can then use these geometries to examine the effect of length on the torque-angular velocity relationship.

Similarly, diabolos of varying radii are created by scaling the diabolo radially, while keeping the length of the diabolo constant. The outer radius, inner radius, and narrow section of the diabolo are updated. The radius scales are shown in table 3. These geometries are used to examine the effect of radius on the torque-angular velocity relationship.

3.1 Effect of length

As shown in figure 10, increasing the length of the diabolo increases the torque exerted on it. The relation between torque and angular velocity remains the same ($\tau = \alpha\omega^{\beta}$) however the values of α and β vary with different diabolo lengths. The value of alpha increases linearly with diabolo length as shown in figure 11 which is based on the calculated values of α in table 2, giving us the relationship

$$\alpha = 8.64 \cdot 10^{-8} \cdot L + 1.39 \cdot 10^{-7} \qquad (14)$$

The value of β stays around 1.6 as shown in figure 12 which is based on the calculations in table 2. There is no strong correlation between β and length which suggests that β remains constant at about 1.6 for all lengths.

Furthermore, a relationship between torque and length can be derived when ω is held constant. The torque exerted on the diabolo increases linearly with diabolo length as shown in figure 13 where the angular velocity is 600 rad/s. We see a similar linear relationship for other angular velocities. The torque on the diabolo can then be expressed as

$$\tau = aL + b \qquad (15)$$

a and b graphed against ω are shown in figures 14 and 15 respectively.

Length Scale (dimensionless)	α (N m)	β (dimensionless)
0.25	1.38E-07	1.613
0.5	1.95E-07	1.580
0.75	2.11E-07	1.592
1	2.41E-07	1.600
1.25	2.47E-07	1.606
1.5	2.62E-07	1.623
1.75	2.80E-07	1.633
2	3.14E-07	1.628

Table 2: α and β as a function of varying length scale from the base diabolo geometry. α increases due to increased contact surface area. β stays around 1.6 for all lengths suggesting length has no effect on β. Length scale is the ratio between varied lengths against base diabolo length.

Radius Scale (dimensionless)	α (N m)	β (dimensionless)
0.25	2.82E-09	1.529
0.5	2.17E-08	1.584
0.75	8.17E-08	1.596
1	2.41E-07	1.599
1.25	4.67E-07	1.618
1.5	8.04E-07	1.658
1.75	1.45E-06	1.665
2	2.21E-06	1.703

Table 3: α and β as a function varying radius from the base diabolo geometry. Both variables increase with radius scale. Radius scale is the ratio between varied radii against base diabolo radius.

Performing a linear regression produces figures 16 and 17 allowing us to calculate the following relations:

$$a = 9.21 \cdot 10^{-8} \cdot \omega^{1.66} \tag{16}$$

$$b = 1.37 \cdot 10^{-7} \cdot \omega^{1.55} \tag{17}$$

3.2 Effect of radius

As shown in figure 18, increasing the radius of the diabolo increases the torque exerted as expected. The general relation between torque and angular velocity remains the same. ($\tau = \alpha\omega^{\beta}$)

The value for α increases as radii increases as shown in figure 19 which is based on table 3. The smoothness of the curve indicates the use of linear regression, producing figure 20. From this, we can conclude that

$$\alpha = 2.27 \cdot 10^{-7} \cdot r^{3.23} \tag{18}$$

The value for β increases linearly with radii as shown in figure 21 which is based on table 3, giving

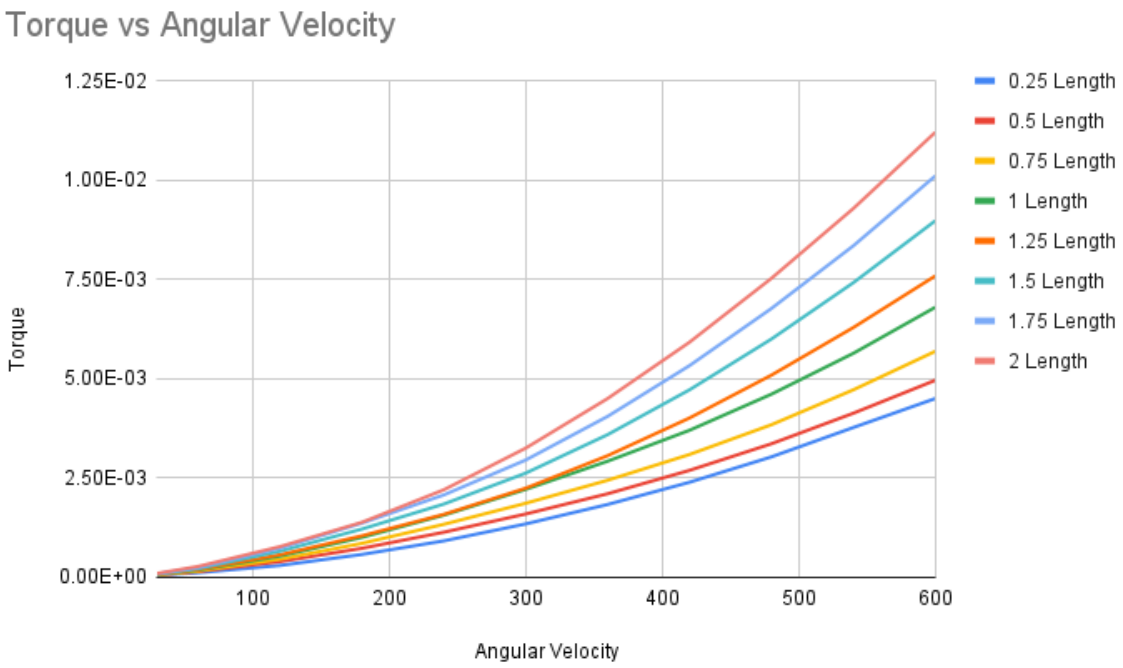

Figure 10: Torque as a function of angular velocity for varying diabolo lengths.

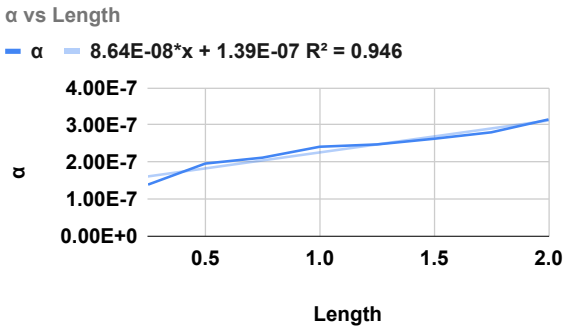

Figure 11: There is a linear relationship between α and diabolo length. α increases from 1.3E-7 to 3.1E-7 as length increases from 0.25 to 2.

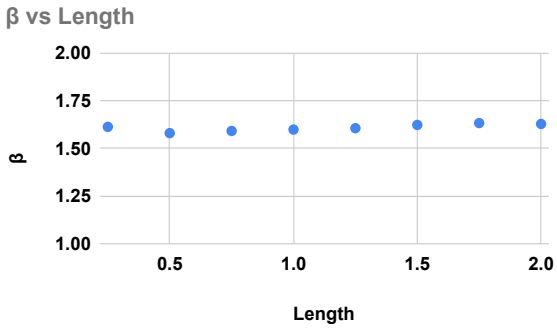

Figure 12: β stays around 1.6 when length scale is varied.

$$\beta = 0.0869r + 1.52 \tag{19}$$

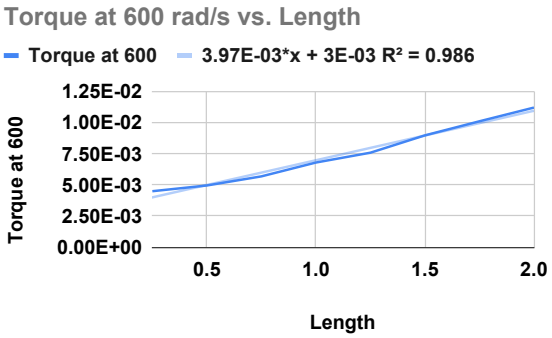

Figure 13: There is a linear relationship between torque and length. The torque increases from 4.49E-3 to 1.12E-2 as length scale increases from 0.25 to 2.

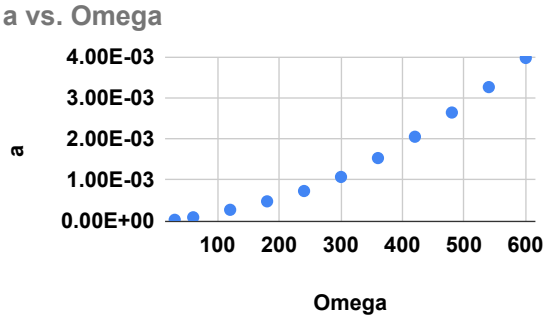

Figure 14: The value of a increases from 2.51E-5 to 3.97E-3 as ω increases from 30 to 600. The shape of the curve suggests the use of linear regression.

A similar relation can be derived between torque and radius when ω is held constant. Figure 23 shows the torque on the diabolo for varying radii when $\omega = 600$ rad/s. After performing a linear regression as shown in figure 22, we see that $\tau = 7.60 \cdot 10^{-3} \cdot r^{3.72}$ or more generally,

$$\tau = ar^b \tag{20}$$

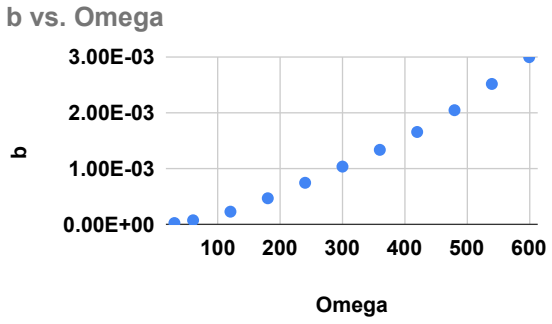

Figure 15: The value of b increases from 2.92E-5 to 3.00E-3 as ω increases from 30 to 600. The shape of the curve suggests the use of linear regression.

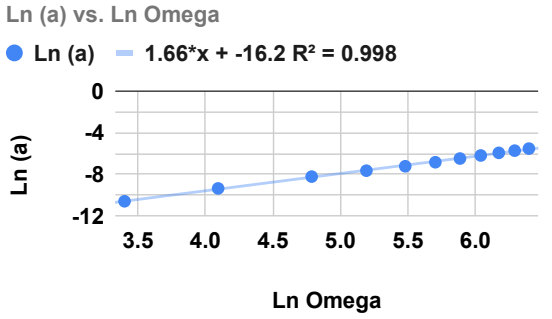

Figure 16: The log scale graph of a and ω produces a straight line with high correlation which gives the relationship $a = 9.21 \cdot 10^{-8} \cdot \omega^{1.66}$.

The values for a and b do not remain constant for varying values of ω. The value of a increases with ω as shown in figure 24. Performing a linear regression gives us figure 25 and the equation

$$a = 3.38 \cdot 10^{-7} \cdot \omega^{1.56} \tag{21}$$

b increases with ω as well however there is no strong correlation between between b and ω with or without a log scale as seen in figure 26.

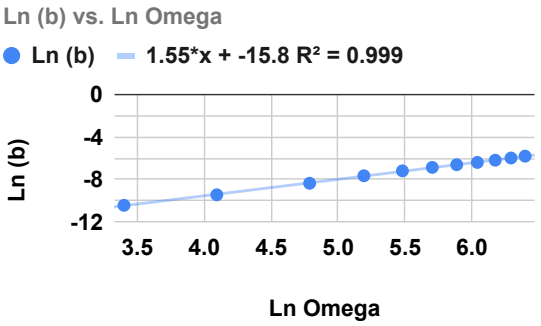

Figure 17: The log scale graph of b and ω produces a straight line with high correlation which gives the relationship $b = 1.37 \cdot 10^{-7} \cdot \omega^{1.55}$.

4 Conclusion and future work

By varying the angular speed of the base diabolo geometry, we have observed a power law relationship between torque and angular velocity $\tau = \alpha\omega^{\beta}$. By further examining the dependence of torque on the shape of the diabolo, we can conclude that both coefficients are functions of the geometry of the diabolo.

The diabolo used in our simulation has a smooth wall which could perform better if we used a dimpled surface to reduce air resistance. We are not aware of any diabolos made of a dimpled surface. It'll be interesting to further investigate the effect of dimpled wall on the aerodynamics of diabolo.

One critical element missing from this work is experimental validation of the dependence found from CFD simulation. We suggest setting up experiments to verify if the predicted torque-angular velocity relationship agrees with observation. One approach is to measure the mechanical power required to sustain a constant angular speed described by equation 22.

$$P = \tau\omega = \alpha\omega^{\beta} \cdot \omega = \alpha\omega^{\beta+1} \tag{22}$$

By measuring the power of motor needed to sustain the diabolo at varying angular velocity, we can then verify if the coefficients α and β agrees with CFD simulation.

A second approach is to measure the angular deaccleration of the diabolo as a result of the viscous torque from air in the spinning diabolo. The measured deacceleration and the rotational inertia of the diabolo yields measured torque which then can be compared with predicted $\tau - \omega$ relationship.

$$\tau = I\frac{d\omega}{dt} = -\alpha\omega^{\beta}$$

$$\frac{d\omega}{dt} = -\frac{\alpha}{I}\omega^{\beta}$$

$$\omega(t) = ((\beta - 1)\frac{\alpha}{I}t)^{\frac{1}{1-\beta}} \tag{23}$$

By measuring how ω of a spinning diabolo slows down and comparing with equation 23, we can experimentally determine α and β then compare with the simulated result from OpenFOAM.

It would be interesting to set up the above experiments using spinning diabolos to measure the dependence of torque on angular velocity and compare it with the result simulated from OpenFOAM. The comparison will help us better understand the strengths and weaknesses of OpenFOAM's result in this study.

References

[Kim] Kim HC, et al, "Three-dimensional flow analysis around a cylinder with dimples", Asia-Pacific congress on sports technology, 2005

[2] Archenbach E., "Experiments on the flow past spheres at very high Reynolds numbers", J Fluid Mech 54, 1972, 565-75

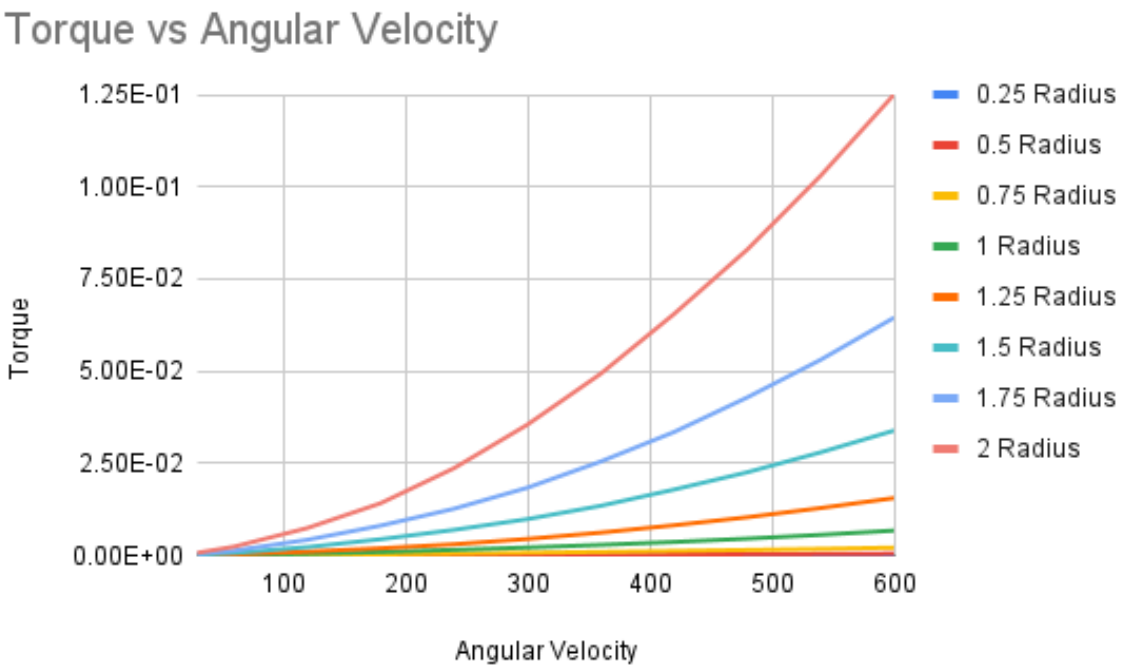

Figure 18: Torque as a function of angular velocity for varying radii.

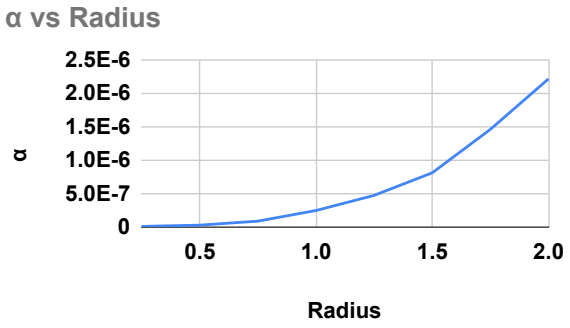

Figure 19: α increases as radius increases.

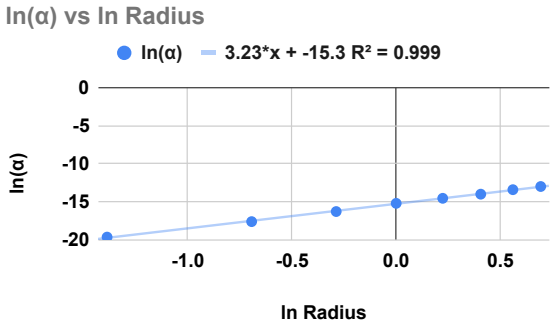

Figure 20: The log scale graph of α and radius produces a straight line.

[3] Taneda S., "Visual observations on the flow past spheres at Reynods numbers between 10^4 and 10^6", J Fluid Mech., 85, 1978, 187-92

[4] Constantinescu GS, et al, "Turbulence modelling applied to flow over a sphere", AIAA J, 41(9), 2003,

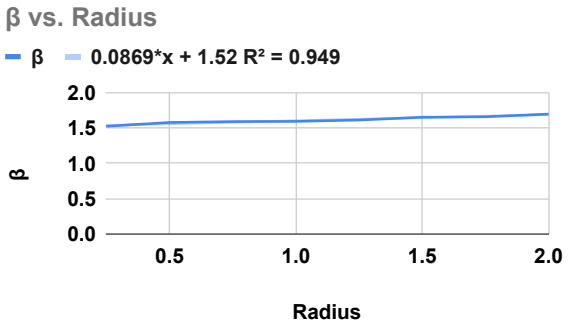

Figure 21: β increases linearly from 1.53 to 1.70 as radius increases from 0.25 to 2 times the base radius.

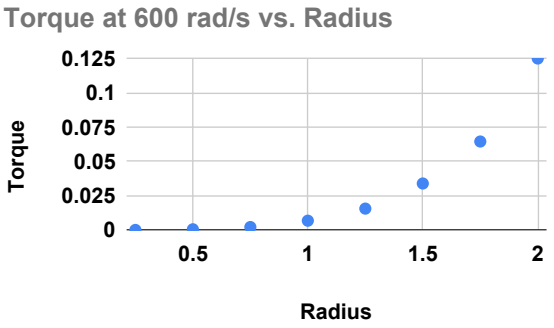

Figure 23: Torque on the diabolo with respect to its radius. The smoothness of the curve indicates the use of linear regression.

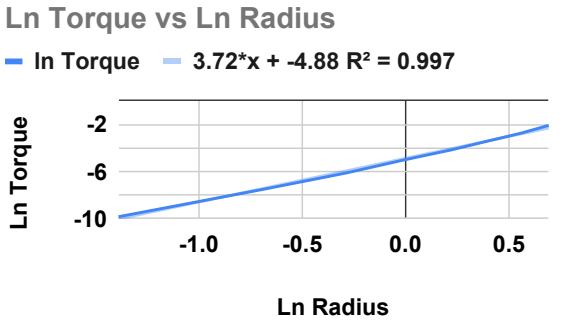

Figure 22: Log scale graph of Torque vs Radius. The value of R squared is close to 1 showing a strong correlation between torque and radius.

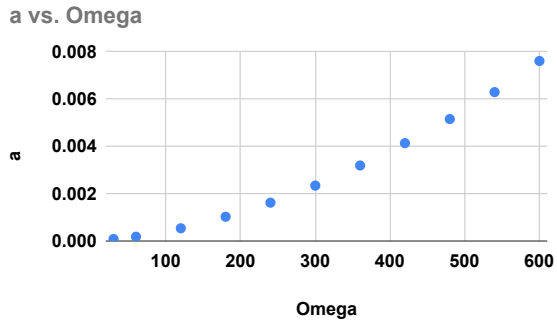

Figure 24: The value of a with respect to Omega.

1733-43

[5] Penrose JMT, et al, "Cricket ball swing: a preliminary analysis using CFD" The engineering of sport, Sheffield, UK, 1996

[6] TIng LL., "Application of CFD technology analysing the 3D aerodynamic behavior of dimpled golf balls", ASME international mechanical engineering congress and exposition, 2002, New Orleans, Louisiana.

[7] Ting LL., "Effect of teardrop shaped dimple design on the golfball aerodynamic performance", ISEA 5th engineering of sport conference, 2004, International Sports Engineering Association.

[8] Aoki K, et al, "Effect of the dimple structure on the flying characteristics and flow patterns of a golf ball", 2004 "ISEA 5th engineering of sport conference. International Sports Engineering Association.

[9] Carre MJ, et al, "The curve kick of a football 2: flight through the air", Sports Eng., 5, 2002, 183-92

[10] Barber S., "The aerodynamics of association footballs", Mechanical engineering, University of Sheffield, 2007

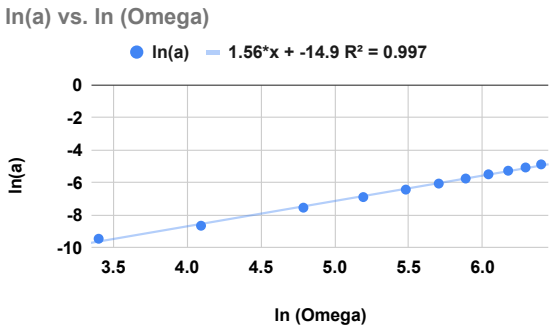

Figure 25: The log scale graph produces a straight line.

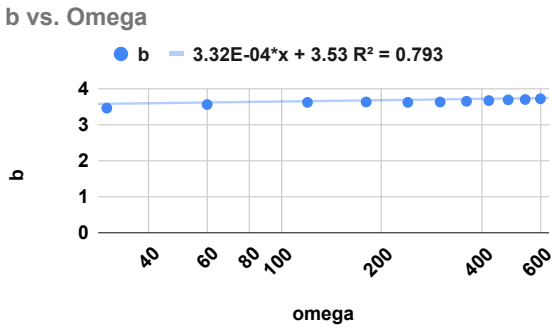

Figure 26: With a R squared value of 0.793, there is a weak correlation between b and omega.

[11] Barber S.,et al, "Sports ball aerodynamics: A numerical study of the erratic motion of soccer balls", Computers Fluids, 38, (2009) 1091-100

[12] Asai T., et al, "A fundamental study on aerodynamics of soccer ball", Proceedings of 83rd Japan society of mechanical engineering conference (Fluid engineering division), 2005

[13] Jasak H., "Error Analysis and Estimation for the Finite Volume Method with applications to Fluid Flows", Direct, M

[14] H. K. Versteeg and W. Malalasekera, An Introduction to Computational Fluid Dynamics: The Finite Volume Method Longman Scientific and Technical, 1995.

[15] J. H. Ferziger and M. Peric´, Computational Methods for Fluid Dynamics Springer, Berlin, 1996.

[16] H. Alan and F. Liu, Computational Fluid Dynamics simulation of a spinning diabolo. Private communication. 2020.

[17] Owen, S. J. 1998. A survey of unstructured mesh generation technology. In Proc. 7th Inter. Mesh. Roundtable, 239–267.

[18] Community, B. O. (2018). Blender - a 3D modelling and rendering package. Stichting Blender Foundation, Amsterdam. Retrieved from http://www.blender.org

[19] `https://www.diabolotricks.com/wii-BabacheFinesse.html`

[20] Henk Kaarle Versteeg, Weeratunge Malalasekera (2007). An Introduction to Computational Fluid Dynamics: The Finite Volume Method.